Numerical Solution of Convection-Diffusion Problems in Irregular Domains Mapped onto a Circle

Makoto Asaba,* Yutaka Asako,† and Hiroshi Nakamura‡
Tokyo Metropolitan University, Tokyo, Japan
and
Mohammad Faghri§
University of Rhode Island, Kingston, Rhode Island 02881

A coordinate transformation methodology has been developed for convection-diffusion problems with an arbitrary solution domain. An algebraic coordinate transformation is used that maps the solution domain onto a circle. The transformed conservation equations are discretized by a control-volume finite difference technique. Sample computations are performed for fully developed flow and heat transfer in a polygonal duct, and for natural convection in a square cavity, to validate the present methodology. The numerical results obtained compared reasonably well, even in the extreme case of a rectangular domain mapped onto a circle.

Nomenclature

a = thermal diffusivity
b = source term
c_p = specific heat
D_h = equivalent hydraulic diameter
e_R, e_θ = unit vectors in R, θ direction
e_η, e_ξ = unit vectors in η, ξ direction
k = thermal conductivity
L = characteristic length
Nu = Nusselt number
n = refers to the number of sides of the polygonal duct
n = unit vector along normal to surface
Pr = Prandtl number
q = heat flux
R,r = radial coordinate: dimensionless and dimensional, respectively
Ra = Rayleigh number, $= g\beta L^3(t_h - t_c)/a\nu$
S = control surface for main control volume
T,t = temperature: dimensionless and dimensional, respectively
t_b = bulk temperature
t_c = cold wall temperature
t_h = hot wall temperature
t_{ref} = reference temperature
Δt = temperature difference
U,u = velocity component in θ direction: dimensionless and dimensional, respectively
V,v = velocity component in r direction: dimensionless and dimensional, respectively
V = velocity vector
U_ξ, V_η = dimensionless velocity component in ξ and η directions
$\bar{w}$ = mean axial velocity
Z,z = axial coordinate: dimensionless and dimensional
α = geometric function, $= 1 + \beta^2$
β = geometric function, $= (1/\delta)(\partial\delta/\partial\xi)$, and also coefficient of thermal expansion
Γ = diffusion coefficient
γ = diffussion term, $= -(1/\eta)(\delta\phi/\delta\xi)$
$\Delta(\theta)$ = dimensionless radius of solution domain
$\delta(\theta)$ = radius of solution domain
δ' = first derivative of δ
δ'' = second derivative of δ
δ''' = third derivative of δ
η = transformed coordinates, $\eta = LR/\delta$
θ = peripheral coordinate
Λ = pseudodiffusion term, $= \beta(\partial\phi/\partial\xi)$
ν = kinematic viscosity
ξ = transformed coordinate, $\xi = \theta$
ρ = density
σ = bulk temperature gradient parameter
Ψ = pseudodiffusion term, $= \beta(\partial\phi/\partial\eta)$
Ω = diffusion term, $= -\alpha\eta(\partial\phi/\partial\eta)$

Received Sept. 19, 1988; revision received Aug. 28, 1989.

*Graduate Student, Department of Mechanical Engineering.
†Associate Professor, Department of Mechanical Engineering.
‡Professor, Department of Mechanical Engineering.
§Professor, Department of Mechanical Engineering and Applied Mechanics.

Introduction

ONE way to solve convection-diffusion problems for fluid flow in and around complex geometries is the utilization of boundary-fitted coordinates in conjuction with a finite volume technique.[1] This method has been widely used in melting and solidification problems (e.g., see Ref. 2).

Faghri et al.[3] proposed an algebraic coordinate transformation that transforms an irregular solution domain onto a rectangle. The solution domains considered were limited to the geometries bounded by one arbitrary curved side and three straight sides. An extension of the work in Ref. 3 for more general domains, which will be mapped onto a circle, is given here. Sample computations will be performed for fully developed flow and heat transfer in polygonal ducts and for the natural convection in a square cavity.

Formulation

Description of the Problem

A schematic view of the type of physical domain being considered is shown in Fig. 1. As seen there, the origin of the coordinate is located in the domain and the distance from this origin to the boundary is a function of θ, which is denoted by $\delta(\theta)$.

Conservation Equations

The governing equations to be considered are the continuity, momentum, and energy equations. Constant thermophysical properties are assumed and viscous dissipation and com-

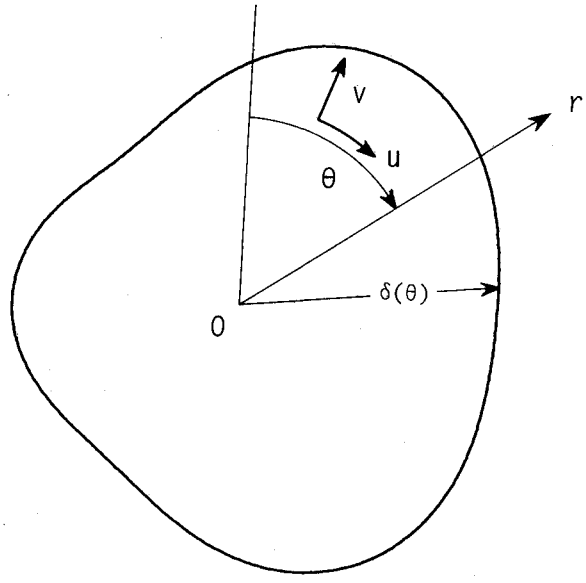

Fig. 1 Illustration of the class of problems under investigation.

pression work are omitted in the energy equation. The following nondimensional variable are used:

$$R = r/L, \qquad U = u/(a/L), \qquad V = v/(a/L)$$

$$P = p/\rho(a/L)^2, \qquad T = (t - t_{\text{ref}})/\Delta t \tag{1}$$

where L, t_{ref} and Δt are reference quantities. Then, upon the introduction of dimensionless variables, the governing equations take the following forms.

Continuity equation:

$$R(\partial V/\partial R) + V + (\partial U/\partial\theta) = 0 \tag{2}$$

Momentum equations:

$$V(\partial V/\partial R) + (U/R)(\partial V/\partial\theta) - U^2/R = -(\partial P/\partial R) + Pr[\nabla^2 V - V/R^2 + (2/R^2)(\partial U/\partial\theta)] \tag{3}$$

$$V(\partial U/\partial R) + (U/R)(\partial U/\partial\theta) - VU/R = -(1/R)(\partial P/\partial\theta) + Pr[\nabla^2 U - U/R^2 + (2/R^2)(\partial V/\partial\theta)] \tag{4}$$

Energy equation:

$$V(\partial T/\partial R) + (U/R)(\partial T/\partial\theta) = \nabla^2 T \tag{5}$$

where $\nabla^2 = (\partial^2/\partial R^2) + (1/R)(\partial^2/\partial R^2) + (1/R^2)(\partial^2/\partial\theta^2)$. The boundary conditions will be specified for the illustrative example discussed later.

Coordinate Transformation

The coordinate transformation methodology in Cartesian coordinates is well documented in an earlier paper.[3] In this paper, the polar coordinates r and θ are transformed into η and ξ coordinates, such that the physical domain bounded by an arbitrary boundary maps onto the circle by the relations:

$$\eta = R/\Delta(\theta), \qquad \xi = \theta \qquad \text{where} \qquad \Delta(\theta) = \delta(\theta)/L \tag{6}$$

In terms of the new coordinates, the solution domain is defined by $0<\eta<1$, and $0<\xi<2\pi$.

Attention will be focused on a new velocity component. Equations (3) and (4) are the components of the vector momentum equation in R and θ directions, respectively. Equation (3) contains the terms that multiply unit vector $\boldsymbol{e}_R$; Eq. (4) contains the terms that multiply unit vector $\boldsymbol{e}_\theta$ in the vector momentum equation. The relation between the orthogonal unit vectors $\boldsymbol{e}_R$, $\boldsymbol{e}_\theta$ and the nonorthogonal unit vectors $\boldsymbol{e}_\eta$, $\boldsymbol{e}_\xi$, as illustrated in Fig. 2, will be obtained first. Since lines of constant ξ coincide with the θ coordinate lines, $\boldsymbol{e}_\eta = \boldsymbol{e}_R$. To determine $\boldsymbol{e}_\xi$, consideration is first given to the unit vector $\boldsymbol{n}$ that is perpendicular to a line of constant η. The gradient of η is normal to a line constant η, such that

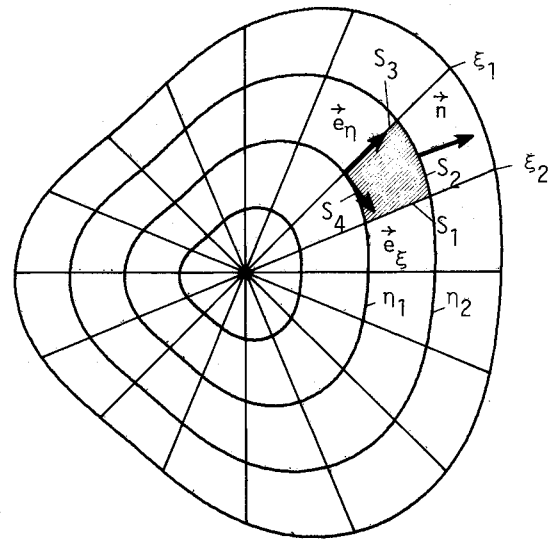

Fig. 2 Constant η and ξ in the physical domain.

$$\boldsymbol{n} = \nabla\eta/|\nabla\eta| = (\boldsymbol{e}_R - \beta\boldsymbol{e}_\theta)/\alpha^{(1/2)} \tag{7}$$

where $\beta = (\partial\delta/\partial\xi)/\delta$, $\alpha = 1 + \beta^2$.

The unit vector $\boldsymbol{e}_\xi$ is normal to $\boldsymbol{n}$, hence

$$\boldsymbol{e}_\xi = (\beta\boldsymbol{e}_R + \boldsymbol{e}_\theta)/\alpha^{(1/2)} \tag{8}$$

The following inverse relations can be obtained directly from $\boldsymbol{e}_\eta = \boldsymbol{e}_R$ and from Eq. (8):

$$\boldsymbol{e}_R = \boldsymbol{e}_\eta, \qquad \boldsymbol{e}_\theta = \alpha^{(1/2)}\boldsymbol{e}_\xi - \beta\boldsymbol{e}_\eta \tag{9}$$

Then any velocity vector $\boldsymbol{V} = (U_\xi, V_\eta)$ can be expressed as

$$\boldsymbol{V} = V_\eta\boldsymbol{e}_\eta + U_\xi\boldsymbol{e}_\xi \qquad \text{or} \qquad \boldsymbol{V} = V\boldsymbol{e}_R + U\boldsymbol{e}_\theta$$

so that

$$V_\eta = V - \beta U, \qquad U_\xi = U\alpha^{(1/2)} \tag{10}$$

A new momentum equation, in which V_η is the primary dependent variable, is introduced by multiplying $-\beta$ by the U momentum equation and by adding it to V momentum equation to obtain

$$V\cdot(\nabla V_\eta + U\nabla\beta) - U^2/R - \beta(UV_\eta/R) - \beta^2U^2/R = -[(\partial P/\partial R) - (\beta/R)(\partial P/\partial\theta)] + Pr[\nabla^2 V_\eta + U\nabla^2\beta + 2\nabla U\nabla\beta] + Pr[-V_\eta/R^2 - (2/R^2)(\partial U/\partial\theta)] - 2Pr\beta[(1/R^2)(\partial V_\eta/\partial\theta) + (U/R^2)(\partial\beta/\partial\theta) + (\beta/R^2)(\partial U/\partial\theta)] \tag{11}$$

This equation will be solved instead of the V momentum equation and the velocity component V in the diffusion terms

of Eq. (4) will be replaced by the new velocity component V_η. Then, Eq. (4) can be rewritten as

$$V\cdot\nabla U + V_\eta U/R + \beta U^2/R = -(1/R)(\partial P/\partial\theta) + Pr\,\nabla^2 U + Pr[-(U/R^2) + (2/R^2)(\partial V_\eta/\partial\theta) + (2\beta/R^2)(\partial U/\partial\theta) + (2U/R^2)(\partial\beta/\partial\theta)] \quad (12)$$

Integral Forms

The momentum Eqs. (11) and (12) and the energy Eq. (5) are integrated over a control volume in physical space bounded by lines of constant η and constant ξ. Such a control volume is illustrated in Fig. 2. Using the divergence theorem, Eq. (11) becomes

$$\int_s (V_\eta\cdot n)V_\eta\,ds - Pr\int_s (n\cdot\nabla V_\eta\,ds = \int_v [-(\partial P/\partial R) + (\beta/R)(\partial P/\partial\theta)]\,dv \int_v -V\cdot(U\nabla\beta)\,dv + Pr\int_v (U\nabla^2\beta + 2\nabla U\nabla\beta)\,dv + \int_v [(U^2/R + \beta(U/R)V_\eta + (\beta U)^2/R)]\,dv - Pr\int_v [(V_\eta/R^2) + (2/R^2)(\partial U/\partial\theta)]\,dv - 2Pr\beta\int_v [(1/R^2)(\partial U/\partial\theta) + (\beta/R^2)(\partial U/\partial\theta) + (U/R^2)(\partial\beta/\partial\theta)]\,dv \quad (13)$$

and Eq. (12) becomes

$$\int_s (V\cdot n)U\,ds - Pr\int_s n\cdot\nabla U\,ds = -\int_v (1/R)(\partial P/\partial\theta)\,dv - \int_v [(UV_\eta/R) + (\beta U^2/R)]\,dv + Pr\int_v [(-U/R^2 + (2/R^2)(\partial V_\eta/\partial\theta) + (2\beta/R^2)(\partial U/\partial\theta) + (2U/R^2)(\partial\beta/\partial\theta)]\,dv \quad (14)$$

and Eqs. (5) and (2) become

$$\int_v (V\cdot n)T\,ds = \int_s n\cdot\nabla T\,ds \quad (15)$$

$$\int_v (\nabla\cdot V)\,dv = \int_s (V\cdot n)\,ds = 0 \quad (16)$$

For the evaluation of the surface integrals, expressions are needed for the surface element ds, the gradient operator ∇, and the unit vector n. To derive these quantities, it is first necessary to consider a formal coordinate transformation from R and θ to η and ξ, where η and ξ have been defined by Eq. (6). The transformation is

$$(\partial/\partial R)_\theta = (1/\Delta)(\partial/\partial\eta)_\xi \quad (17a)$$

$$(\partial/\partial\theta)_R = -\eta\beta(\partial/\partial\eta)_\xi + (\partial/\partial\xi)_\eta \quad (17b)$$

To facilitate the evaluation of the surface integrals that appear in Eqs. (13–16), reference may be made to the shaded control volume of Fig. 2. As suggested there, the surface integral may be subdivided into a sum of four surface integrals over the segments S_1, S_2, S_3, and S_4. For surface 1, $n = e_\theta$, $V\cdot n = U$; also, ξ = constant along S_1. Therefore, an element of surface area can be expressed as

$$ds = dR = \Delta d\eta \quad (18)$$

For surface 2,

$$n = (e_R - \beta e_\theta)/\alpha^{(1/2)}, \qquad V\cdot n = V_\eta/\alpha^{(1/2)} \quad (19)$$

and

$$ds = [dR^2 + (R\,d\theta)^2]^{(1/2)} = R(\beta^2+1)^{(1/2)}\,d\xi = \alpha^{(1/2)}R\,d\xi \quad (20)$$

For surface S_3 and S_4, ds is identical to those for S_1 and S_2, with the exception that the outward normal n has the opposite sign. The volume integrals appearing on the right-hand side of Eqs. (11) and (12) can now be evaluated. The volume element dv can be written as

$$dv = R\,dR\,d\theta = \Delta^2\eta\,d\eta\,d\xi \quad (21)$$

The standard form of the ∇ operator in cylindrical coordinates is

$$\nabla = (\partial/\partial R)\,e_R + (1/R)(\partial/\partial\theta)\,e_\theta \quad (22)$$

which, after substitution for $\partial/\partial R$ and $\partial/\partial\theta$ from Eqs. (17), becomes

$$\nabla = (1/\Delta)(\partial/\partial\eta)\,e_R + (1/\eta\Delta)[(\partial/\partial\xi) - \eta\beta(\partial/\partial\eta)]\,e_\theta \quad (23)$$

The evaluation of the all surface integrals and the volume integrals in Eqs. (13–16) can be performed by using Eqs. (17–23) in the same manner as described by Faghir et al.[3] Because of the similarities among Eqs. (13–15), it is possible to rewrite them in a compact form by introducing the abbreviations

$$\int_1 [U\phi\Delta + \Gamma(\gamma+\Psi)]\,d\eta - \int_3 [U\phi\Delta + \Gamma(\gamma+\Psi)]\,d\eta + \int_2 [V_\eta\phi\Delta\eta + \Gamma(\Omega+\Lambda)]\,d\xi - \int_4 [V_\eta\phi\Delta\eta + \Gamma(\Omega+\Lambda)]\,d\xi = b \quad (24)$$

where ϕ stands for U, V_η, or T, and Γ is the diffusion coefficient that is equal to Pr for the momentum equations and equal to one for the energy equation. The variables Ω, γ, Λ, and Ψ are abbreviations that are defined as

$$\Omega = -\alpha\eta(\partial\phi/\partial\eta), \qquad \gamma = -(1/\eta)(\partial\phi/\partial\xi)$$

$$\Lambda = \beta(\partial\phi/\partial\xi), \qquad \Psi = \beta(\partial\phi/\partial\eta) \quad (25)$$

The term b in V_η and U momentum equations is obtained from the right-hand side of Eqs. (13) and (14), respectively, and is zero for the energy equation.

Discretization

Equation (24) is discretized by the widely known control volume scheme of Patankar.[4] The pseudodiffusion terms in Eq. (24) are included in the source term. The staggered grids are used such that the grid points for temperature are located at the center of the main control volumes and the grid points for the velocity components are located on the sides of the main control volume. As a result of coordinate transformation, additional terms will arise in the transformed equations. The power law scheme[4] is used to discretize the equations. However, the accuracy of the power law scheme is identical to the standard second-order central difference scheme in the case of conduction problems. The discretized equations are solved by using line-by-line method.[5] The pressure and the velocity are linked by the SIMPLE algorithm.[5] It is well known that the discretization of the differential equation causes false diffusion depending on the Peclet number. A detailed discussion of false diffusion has been given in a book by Patankar.[5]

Sample Computations

Heat Transfer in Fully Developed Region of Polygonal Duct

The first example problem deals with the fully developed laminar flow and heat transfer for regular polygonal ducts with constant wall temperature. A summary of the literature on this problem has been brought together by Shah and London.[6] The cross section of the duct is shown in Fig. 3. The thermal boundary condition is assumed to be uniform temperature, both axially and peripherally. This is the T boundary condition of Shah and London.[6] As seen in this figure, the origin of the coordinate is located at the center of the cross section, and the distance from the origin to the walls is denoted by $\delta(\theta)$. The geometry of the duct is specified by length L and parameter n. The shaded area in the figure is the solution domain. Because of symmetry, it is sufficient to confine the solution domain to only $(1/n)$th of the cross section. The expression for $\delta(\theta)$ is as follows:

$$\delta(\theta) = 0.5L/[\tan(\pi/n)\cos(C\pi/n + \theta)] \tag{26}$$

where C is a constant and changes with θ.

$$0<\theta<\pi/n \qquad C = 0 \tag{27a}$$

$$\pi/n<\theta<2\pi/n \qquad C = -2 \tag{27b}$$

The governing equations to be considered here are the momentum and energy equations. Constant thermophysical properties are assumed. Using the following nondimensional variables

$$R = r/D_h, \qquad Z = z/(D_h/Re), \qquad W = w/\bar{w}$$

$$P = p/\rho\bar{w}^2, \qquad T = (t-t_w)/(t_b-t_w) \tag{28}$$

Thus, the governing equations take the following forms:

$$0 = -(\partial P/\partial Z) + \nabla^2 W \tag{29}$$

$$0 = \nabla^2 T - PrWT\sigma \tag{30}$$

where

$$\sigma = (\mathrm{d}t_b/\mathrm{d}Z)/(t_b-t_w) \tag{31}$$

which is the parameter arising from the assumptions of the T boundary condition. This value is determined as part of the solution process from the identity of $\int TW\,\mathrm{d}A = \int W\,\mathrm{d}A$. It is obvious from the Eqs. (29) and (30) that the problem to be considered reduces to the diffusion problem.

The friction factor f is defined as

$$f = -(2D_h)(\mathrm{d}p/\mathrm{d}z)/\rho\bar{w}^2 = 2(\mathrm{d}P/\mathrm{d}Z)/Re \tag{32}$$

In the fully developed region, the friction factor becomes inversely proportional to the Reynolds number, and $(fRe)_{f.d.}$ becomes independent of z and equal to $2(\mathrm{d}P/\mathrm{d}Z)$.

The heat flux from the walls can be expressed as

$$q = c_p\dot{m}\,(\mathrm{d}t_b/\mathrm{d}z)/(nL) = \rho c_p\bar{w}\,(D_h/4)(\mathrm{d}t_b/\mathrm{d}z) \tag{33}$$

where the $\dot{m}$ is the mass flow rate, n refers to the number of sides of polygonal duct, and nL represents the perimeter. The Nusselt number, based on the hydraulic diameter, can be expressed as

$$Nu = qD_h/[k(t_w-t_b)] = -Pr\sigma/4 \tag{34}$$

The computations were performed for the triangular, rectangular, pentagonal, and hexagonal ducts. To investigate the grid size effect on the friction factor and the Nusselt number, the computations were performed with various numbers of grid points. The computer friction factor and Nusselt number are listed in Tables 1 and 2, respectively. Shih[7] obtained the friction factor and the Nusselt number values for the fully developed region of regular polygonal ducts. Shih's results[7] are also listed in these tables. The error indicates the

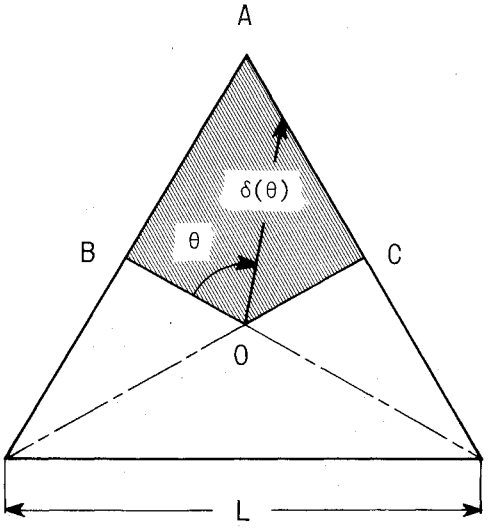

Fig. 3 Schematic diagram of cross section of triangular duct.

Table 1 Fully developed value of $(fRe)_{f.d.}$

n	Grid points	$(fRe)_{f.d.}$	Error, %
3	48×36	54.845	2.90
	78×36	54.317	1.91
	178×36	53.782	0.90
	Shih[7]	53.3	—
4	48×36	57.653	1.31
	78×36	57.372	0.82
	148×36	57.145	0.42
	Shih[7]	56.910	—
5	48×36	59.385	0.74
	78×36	59.216	0.45
	158×36	59.072	0.21
	Shih[7]	58.948	—
6	48×36	60.508	0.48
	78×36	60.390	0.24
	158×36	60.290	0.12
	Shih[7]	60.216	—

Table 2 Fully developed Nusselt number of T boundary

n	Grid points	Nu	Error, %
3	48×36	2.611	5.27
	78×36	2.570	4.04
	178×36	2.530	2.43
	Shih[7]	2.47	—
4	48×36	3.033	1.91
	78×36	3.013	1.23
	148×36	2.996	0.66
	Shih[7]	2.976	—
5	48×36	3.243	0.46
	78×36	3.231	0.09
	158×36	3.221	−0.20
	Shih[7]	3.228	—
6	48×36	3.363	0.40
	78×36	3.355	0.16
	158×36	3.349	−0.04
	Shih[7]	3.35	—

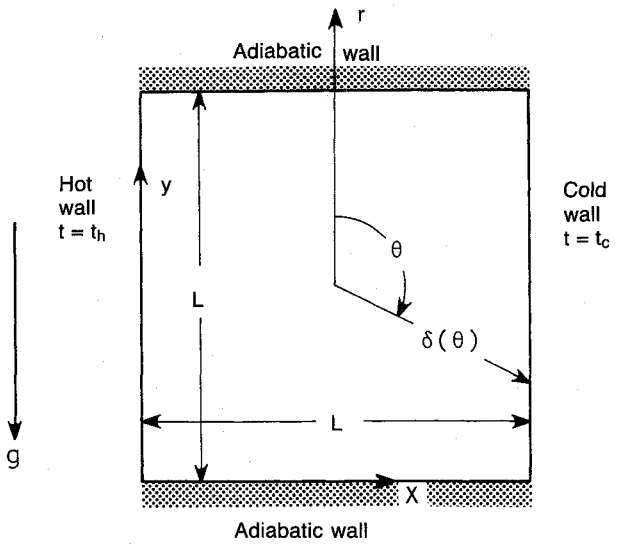

Fig. 4a Schematic diagram of square cavity.

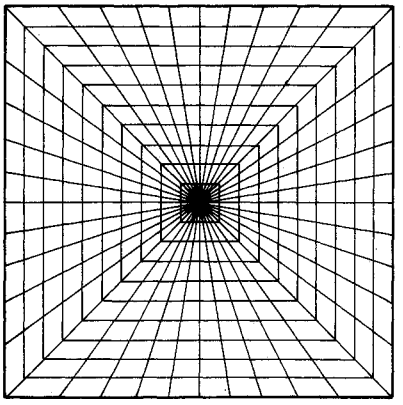

Fig. 4b Typical control-volume distribution.

deviation from Shih's values.[7] As seen from these tables, the percentage error decreases with increasing number of grid points. This tendency is accentuated for pentagonal and hexagonal ducts.

Natural Convection in a Square Cavity

The second example problem deals with the two-dimensional natural convection in a square cavity of side L with differentially heated vertical walls, as shown in Fig. 4a. One side wall is heated at temperature t_h, and the opposite wall is cooled at temperature t_c. The top and bottom walls are thermally insulated. The velocity components are zero on the boundaries. This problem is a well-known bench mark numerical solution.[8] As seen from the figure, the origin of the coordinate is located at the center of the cavity. The distance from the origin to the walls, $\delta(\theta)$, is given by

$$\delta(\theta) = 0.5L/\sin(C\pi - \theta) \tag{35}$$

where C is a constant and changes with θ.

$$0<\theta<\pi/4 \qquad C = 0.5 \tag{36a}$$

$$\pi/4<\theta<(3/4)\pi \qquad C = 1.0 \tag{36b}$$

$$(3/4)\pi<\theta<(5/4)\pi \qquad C = 1.5 \tag{36c}$$

$$(5/4)\pi<\theta<(7/4)\pi \qquad C = 2.0 \tag{36d}$$

$$(7/4)\pi<\theta<2\pi \qquad C = 2.5 \tag{36e}$$

and its derivatives can be easily obtained.

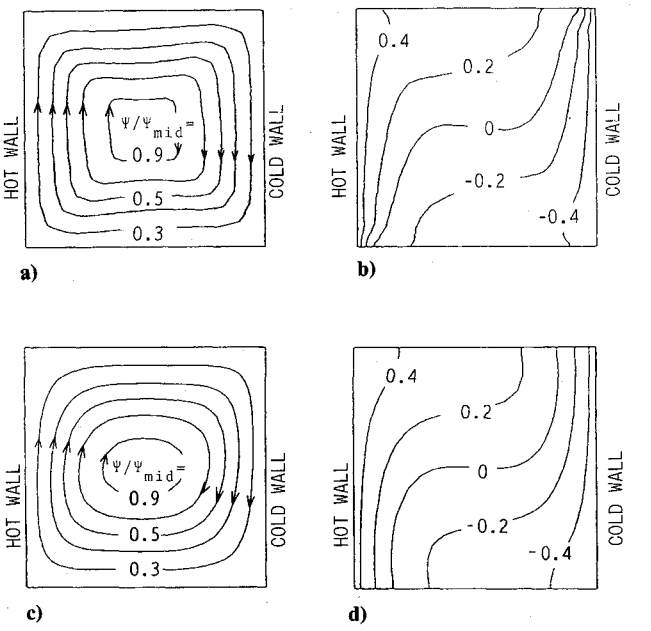

Fig. 5 Streamlines and isotherms obtained from the coordinate transformation (40 × 22) [a) and b)] and from the x-y coordinate computation (22 × 22) [c) and d)].

Using the Boussinesq approximation, the governing equations of this problem are Eqs. (2–5), with the extra source terms that are derived from the buoyancy force. These terms are $(-RaPrT\cos\theta)$ and $(-RaPrT\sin\theta)$, which are added to Eqs. (3) and (4), respectively.

Computations were performed for $Ra = 10^3$, 10^4, and 10^5, with grid points of (40 peripheral) × (12 radial) and for $Pr = 0.71$. These grid points are distributed uniformly. A typical main control-volume distribution is illustrated in Fig. 4b. The average temperature $t_m = (t_h + t_c)/2$ is selected for the characteristics temperature t_{ref}. The temperature difference between the two walls, $(t_h - t_c)$, is selected as the characteristic temperature difference Δt, so that the nondimensional temperature of the hot wall T_h is 0.5 and that of cold wall T_c is -0.5. The average heat flux from the hot wall, q, can be expressed as

$$q = -\left(\frac{k}{L}\right)\int_0^L \left(\frac{dt}{dx}\right) dy = -\left(\frac{k}{L}\right)(t_h - t_c) \times \int_{5\pi/4}^{7\pi/4} \alpha\left(\frac{\partial T}{\partial \eta}\right) d\xi \tag{37}$$

The average Nusselt number based on the characteristic length L is defined as

$$Nu = \frac{qL}{k(t_h - t_c)} = \int_{5\pi/4}^{7\pi/4} \alpha\left(\frac{\partial T}{\partial \eta}\right) d\xi \tag{38}$$

Supplementary runs based on the orthogonal x, y coordinates were also performed for the comparison. The grid points were (22 × 22), which are distributed uniformly.

The representative streamline and isotherm maps obtained from coordinate transformation solutions for $Ra = 10^4$ are shown in Figs. 5a and 5b. The results of the computation based on the orthogonal x, y coordinates are also shown in Figs. 5c and 5d for comparison. The deviation of streamlines near the corners can be seen from these figures.

The representative horizontal velocity profile on the vertical plane of $x/L = 0.5$ is shown in Fig. 6 for $Ra = 10^4$. This vertical plane is located at the midpoint between the hot and the cold walls. The representative vertical velocity profile on

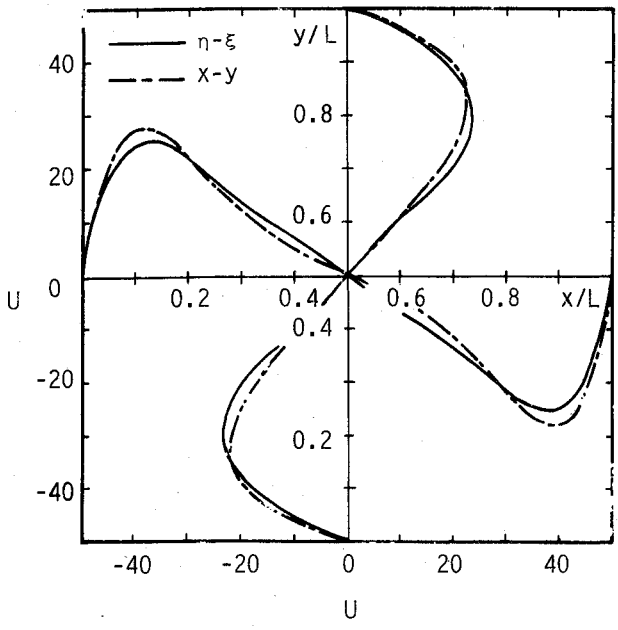

Fig. 6 Comparisons of velocity distributions.

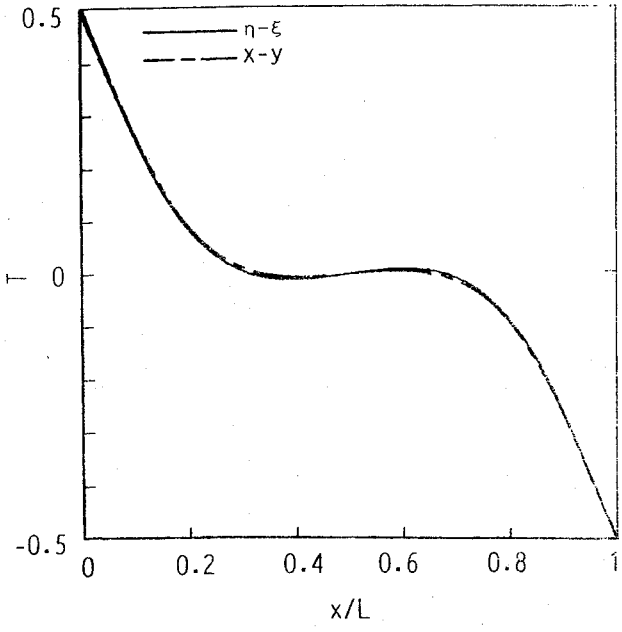

Fig. 7 Comparisons of temperature distribution at $y/L = 0.5$.

the horizontal plane of $y/L = 0.5$ is also shown in the same figure. The solid lines indicate the results of the computation based on the coordinate transformation methodology, and the dashed lines indicate the results of the computation based on the x, y orthogonal coordinate. As seen from the figure, the solid lines and the dashed lines almost coincide with each other.

The representative temperature profile on the horizontal plane of $y/L = 0.5$ is shown in Fig. 7 for $Ra = 10^4$. The solid line indicates the results based on the coordinate transformation methodology, and the dashed line indicates the results based on the x, y orthogonal coordinate. As seen from the figure, the solid lines and the dashed lines almost coincide with each other.

Nusselt number results are listed in Table 3. Results of the supplementary runs based on x-y coordinates are also listed in the table. De Vahl Davis[8] performed two computations with fine and coarse meshes and calculated the extrapolated solution from these two original solutions. De Vahl Davis' extrapolated values are also listed in the same table.

Table 3 Nusselt number values

	Rayleigh number		
	10^3	10^4	10^5
η-ξ coordinates	1.219	2.398	4.900
x-y coordinates	1.123	2.300	4.902
de Vahl Davis[8]	1.118	2.238	5.505

Table 4 Grid size effect on the Nusselt number

Grid points	*Nu*
40×12	2.398
40×22	2.371
40×27	2.365
de Vahl Davis[8]	2.238

Table 5 Effect of omission of the derivatives on Nusselt number

Omitted derivatives	*Nu*
a) $\Delta''' = \Delta'' = \Delta' = 0$	2.247
b) $\Delta''' = \Delta'' = 0$	2.414
c) $\Delta''' = 0$	2.351
no-omission	2.398
de Vahl Davis[8]	2.238

To investigate the grid size effect on the Nusselt number, supplementary computations were performed for $Ra = 10^4$ with fine meshes. Number of grid points are (40 peripheral × 22 radial) and (40 × 27). The Nusselt number results are listed in Table 4. The Nusselt number found by the present methodology with fine mesh approaches de Vahl Davis' extrapolated value.

Equations (13) and (14) involve the first, second, and third derivatives of $\Delta(\theta)$. In many works for the solidification problems, in which the boundary-fitted coordinate transformation methodology was adopted, the derivatives of $\Delta(\theta)$ were often neglected in the computation,[9] because of the gradual sloped of interface boundary. Therefore, to investigate the effect of the omitted derivatives, supplementary computations were performed with the following assumptions:

$$\partial\Delta/\partial\xi = 0, \qquad \partial^2\Delta/\partial\xi^2 = 0, \qquad \partial^3\Delta/\partial\xi^3 = 0$$

$$\partial^2\Delta/\partial\xi^2 = 0, \qquad \partial^3\Delta/\partial\xi^3 = 0$$

$$\partial^3\Delta/\partial\xi^3 = 0$$

The number of grid points was (40 × 22) and the Rayleigh number was $Ra = 10^4$. The Nusselt number results are listed in Table 5. It is noteworthy that the effect of the omitted derivatives on the Nusselt number were small.

Concluding Remarks

The development of a coordinate transformation methodology for convection-diffusion problems that maps the arbitrary domain onto a circle is presented. Sample computations were performed for the heat transfer in a fully developed region of a polygonal duct and for the natural convection in a two-dimensional square cavity. Comparisons were made with the available values.

References

[1]Saitoh, T., "Numerical Method for Multi-Dimensional Freezing Problem in Arbitrary Domains," *ASME Journal of Heat Transfer*, Vol. 100, No. 2, 1978, pp. 294-299.

[2]Sparrow, E. M., Patankar, S. V., and Ramadhyani, S., "Analysis of Melting in the Presence of Natural Convection in the Melt Region," *ASME Journal of Heat Transfer*, Vol. 99, No. 4, 1977, pp. 520–526.

[3]Faghri, M., Sparrow, E. M., and Prata, A. T., "Finite-Difference Solution of Convection-Diffusion Problems in Irregular Domains, Using a Nonorthogonal Coordinate Transformation," *Numerical Heat Transfer*, Vol. 7, No. 2, 1984, pp. 183–209.

[4]Patankar, S. V., "A Calculation Procedure for Two-Dimensional Elliptic Situation," *Numerical Heat Transfer*, Vol. 4, No. 4, 1981, pp. 409–425.

[5]Patankar, S. V., *Numerical Heat Transfer and Fluid Flow*, McGraw-Hill, New York, 1980.

[6]Shah, R. K., and London, A. L., *Laminar Flow Forced Convection in Ducts*, Academic, New York, 1978.

[7]Shih, F. S., "Laminar Flow in Axisymmetric Conduits by a Rational Approach," *Canadian Journal of Chemical Engineering*, Vol. 45, No. 5, 1967, pp. 285–294.

[8]de Vahl Davis, G., "Natural Convection of Air in a Square Cavity: A Bench Mark Numerical Solution," Univ. of New South Wales School of Mechanical and Industrial Engineering, Australia, Rept. 1982/FMT/2, 1982.

[9]Sparrow, E. M., and Ohkubo, Y., "Numerical Analysis of Two-Dimensional Transient Freezing Including Solid-Phase and Tube-Wall Conduction and Liquid-Phase Natural Convection," *Numerical Heat Transfer*, Vol. 9, No. 1, 1986, pp. 59–77.